Trajectory Based Time-Resolved Mechanism for Benzene Reductive Elimination from Cyclopentadienyl Mo/W Phenyl Hydride Complexes

Joshua I. Wheeler, Anthony J. Schaefer, and Daniel H. Ess*

Department of Chemistry and Biochemistry, Brigham Young University, Provo, Utah, 84604, United States

Abstract

Calculated potential energy structures and landscapes are very often used to define the sequence of reaction steps in an organometallic reaction mechanism and interpret kinetic isotope effect (KIE) measurements. Underlying most of this structure-to-mechanism translation is the use of statistical rate theories without consideration of atomic/molecular motion. Here we report direct dynamics simulations for an organometallic benzene reductive elimination reaction where nonstatistical intermediates and dynamic-controlled pathways were identified. Specifically, we report single spin state as well as mixed spin state quasiclassical direct dynamics trajectories in the gas phase and explicit solvent for benzene reductive elimination from Mo and W bridged cyclopentadienyl phenyl hydride complexes ($[Me_2Si(C_5Me_4)_2]M(H)(Ph)$, M = Mo and W). Different from the energy landscape mechanistic sequence, the dynamics trajectories revealed that after the benzene C-H bond forming transition state (often called reductive coupling) σ-coordination and π-coordination intermediates are either skipped or circumvented and that there is a direct pathway to forming a spin flipped solvent caged intermediate, which occurs in just a few hundred femtoseconds. Classical molecular dynamics simulations were then used to estimate the lifetime of the caged intermediate, which is between 200-400 picoseconds. This indicates that if the η^2-π-coordination intermediate is formed it occurs only after first formation of the solvent caged intermediate. This dynamic mechanism intriguingly suggests the possibility that the solvent caged intermediate rather than a coordination intermediate is responsible (or partially responsible) for the inverse KIE value experimentally measured for W. Additionally, this dynamic mechanism prompted us to calculate the k_H/k_D KIE value for the C-H bonding forming transition states of Mo and W. Surprisingly, Mo gave a normal value while W gave an inverse value, albeit small, due to a much later transition state position.

Introduction

The translation of calculated potential energy surface structures and intrinsic reaction coordinate (IRC)[1] pathways to organometallic reaction mechanisms[2] is very common and often the basis for interpreting experimental measurements, such as kinetic isotope effect (KIE) values.[3] Underlying most of this translation is the use of statistical rate theories, such as transition state theory.[4,5,6] However, there are now several recognized situations when the use of statistical rate theories for interpretation of reaction mechanisms can be incomplete or incorrect without consideration of atomic/molecular motion,[7,8,9] and these nonstatistical situations have often been identified with direct[10,11] molecular dynamics trajectories.[12,13,14,15,16,17] Examples of nonstatistical situations include reactions with non-IRC motion (which can sometimes lead to so-called entropic intermediates[18,19,20]), reactions with pathway splitting (e.g. bifurcation/multifurcation),[21,22] and reactions with intermediates that have shorter-than-expected lifetimes due to a lack of complete intramolecular vibrational energy redistribution (IVR).[23]

While these nonstatistical situations have been identified in several different types of organic reactions[24] (e.g. substitution,[25,26,27,28,] addition,[29,30,31] pericyclic,[32,33] and rearrangement[34,35,36,37,38,39]) it is only recently that they have begun to be discovered in organometallic reactions.[40] Examples include dynamic merging of reaction steps in alkene hydrogenation by a Ru-hydride,[41] reaction pathway bifurcation[42,43] in Rh-carbene,[44,45,46] Au-vinylidene,[47] and Au-carbene[48] reactions, and roaming/unexpected intermediates during Pd transmetalation[49] and Ni cross-coupling reactions.[50]

Over the past few years our group has pioneered identifying and understanding these dynamic effects in organometallic reactions using quasiclassical direct dynamics trajectory calculations,[40] which

provides time-resolved atomic motion details during reactive collisions. Most germane to the current work, direct dynamics trajectories revealed that during the reaction between $Cp(PMe_3)_2Re$ and ethylene there can be direct formation of the Re-vinyl hydride product that either skips or avoids both σ-coordination and π-coordination intermediates, despite their location on the reaction pathway potential energy surface.[51] Our quasiclassical trajectories also demonstrated multiple non-IRC reaction pathway connections for the isomerization of [Tp(NO)(PMe_3)W(η^2-benzene)] and [Tp(NO)(PMe_3)W(H)(Ph)] isomers.[52] Trajectories showed that the weak benzene C-H σ-complex and surrounding vicinity provide a pathway branching hub during reductive coupling/oxidative cleavage and π coordination. Additionally, these trajectories showed that there can be direct benzene elimination from [Tp(NO)(PMe_3)W(H)(Ph)] without the requirement of η^2-coordination.

The possibility that C-H σ-coordination and π-coordination structures can either be skipped or be nonstatistical intermediates (i.e. there is a lack of complete IVR and have a shorter than anticipated lifetime) prompted us to investigate the dynamics of reactions where these weak coordination intermediates have been proposed and are key for the interpretation of experimentally measured kinetic values. Parkin reported in-depth kinetic experiments for the reductive elimination of benzene from Mo and W bridged cyclopentadienyl phenyl hydride complexes ($[Me_2Si(C_5Me_4)_2]M(H)(Ph)$, M = Mo (**1Mo**), W (**1W**); Figure 1a).[53] Comparison of rate constants for benzene reductive elimination of $[Me_2Si(C_5Me_4)_2]M(H)(C_6H_5)$ versus $[Me_2Si(C_5Me_4)_2]M(D)(C_6D_5)$ gave a normal k_H/k_D KIE value of 1.1 for Mo (80 °C) and inverse value of 0.6 for W (182 °C). The difference between normal versus inverse values was rationalized based on a rate limiting first reaction step involving C-H bond formation (reductive coupling) for Mo and generation of an intermediate followed by a rate limiting benzene dissociation second step for W. For W, Parkin also reported a singlet spin state B3LYP potential energy landscape and mechanistic sequence of metal-phenyl hydride **1** conversion to the C-H σ-coordination intermediate **2** and then to the π-coordination intermediate **3** (Figure 1a).[53] The implication of the energy landscape is that **2** and **3** are formed during benzene reductive elimination directly from the reductive coupling step and they are the key intermediates along with a barrier for dissociation that is responsible for the interpretation of the inverse KIE value.

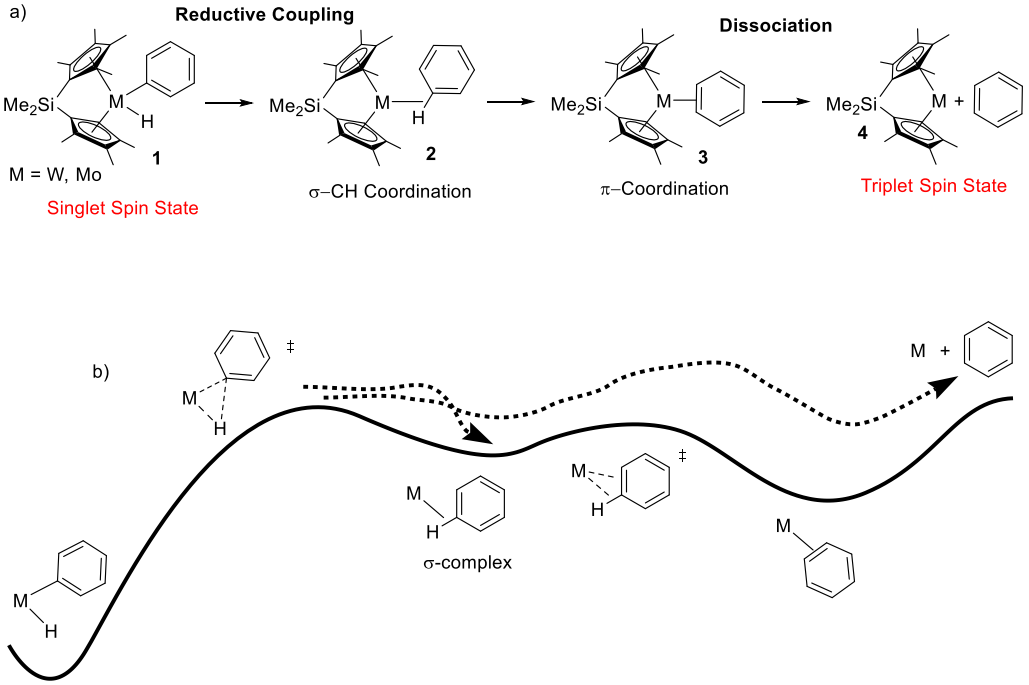

Figure 1. a) Outline of reductive elimination reaction steps for $[Me_2Si(C_5Me_4)_2]M(H)(Ph)$ complexes (M = W and Mo). b) Outline of potential energy surface for benzene reductive elimination and possible reaction trajectory outcomes (dotted arrows).

Our own replication and inspection of this static DFT landscape showed that the C-H σ-coordination structure is in an extremely shallow energy well (~1 kcal/mol) and possibly a nonstatistical intermediate. The implication of a nonstatistical intermediate is that there might be dynamic pathways that either skate through or skip this intermediate and the π-coordination intermediate and lead directly to benzene elimination (Figure 1b). Also important, there is the possibility for singlet to triplet spin state crossover during reductive elimination because the $[Me_2Si(C_5Me_4)_2]M$ structure (**4**) is likely to have a triplet spin ground state while all the other structures likely have a singlet spin ground state, which was previously highlighted by Parkin for methane reductive elimination.[54] Therefore, we used direct dynamics trajectories in the gas phase and explicit solvent with both singlet spin state and a mixed singlet/triplet spin state to examine the time-resolved reaction mechanism of benzene reductive elimination from **1Mo** and **1W**.

For both the Mo and W metal centers, and in both gas phase and explicit benzene solvent, trajectories begun at the transition state for forming the C-H bond (reductive coupling) showed very fast traversal through (100-500 femtoseconds (fs)) and no stopping at the C-H σ-coordination and η^2-π-coordination structures resulting in what is best described as a spin flipped solvent caged intermediate. This dynamical mechanism that was not anticipated from the potential energy surface with fully optimized intermediates couples C-H bond formation with benzene elimination inside the solvent cage. Classical molecular dynamics simulations with a bespoke force field were then used to estimate the lifetime of the caged intermediate, which suggests benzene dissociation across the solvent cage occurs between 200-400 picoseconds (ps). This suggests that if the η^2-π-coordination intermediate **3** is formed during the overall reductive elimination process it occurs only after first formation of the solvent caged intermediate. Alternatively, there is the intriguing possibility that even if the η^2-π-coordination intermediate **3** is not formed that the rate limiting step for W involves the energy of the solvent caged intermediate to undergo exchange with solvent. This time-resolved reaction mechanism prompted us to calculate the k_H/k_D KIE values at the reductive coupling/C-H forming transition state. This showed that the C-H forming transition state provides a normal KIE value for Mo and an inverse value for W, which reveals that the same transition state can give rise to qualitatively different KIE values, however, it is likely that for W the combination of the reductive coupling transition state and benzene penetration through the solvent cage combine to give the observed inverse value.

Methods

For construction of the singlet and triplet potential energy surfaces, structures were located using unrestricted DFT calculations in Gaussian 16[55] with an ultrafine integration grid. All structures (unless noted) were optimized using the M06[56] density functional with the 6-31G**[57][LANL2DZ[58] for W and Mo] basis set. This functional was selected because it generally has solid performance for second-row and third-row transition metal complexes. Stationary points were confirmed as energy minima or saddle points using vibrational frequency analysis and connections were confirmed with IRC calculations.[1] Frequency calculations and thermochemical corrections were done at the experimental temperatures (80 °C for Mo and 182 °C for W).[53] Minimum energy crossing points (MECPs) were located using our MECPro program,[59] which is a variant of Harvey's MECP optimizer program.[60] Briefly, an MECP corresponds to a structure with identical unrestricted singlet and triplet energies. This structure represents a possible (and likely) spin crossover point during a reaction mechanism.

Gas-phase quasiclassical direct dynamics trajectories were initialized at the reductive coupling transition state where the C-H bond is formed. Trajectories were launched in the forward and reverse direction. Initial velocities were obtained through local mode sampling and include zero-point energy and thermal vibrational energy at 80 °C for Mo and 182 °C for W. All gas phase trajectories were performed in Gaussian 16 with unrestricted M06/6-31G**[LANL2DZ for W and Mo] on the singlet surface (allowing for a open-shell solution) with a time step of approximately 0.75 fs. Spin crossover was not considered in gas phase trajectories.

For explicit solvent trajectories, the M06 optimized C-H bond forming reductive coupling transition-state structure was surrounded by a box of 72 benzenes (the experimental solvent) with a volume of 25 $Å^3$. The Packmol program was used to generate the initial solvent configuration. Equilibration of solvent for >2 ps around the transition-state structures (kept frozen) was carried out in the CP2K[61] program with periodic boundary conditions using a velocity-Verlet algorithm and xTB to calculate forces. Canonical sampling through a velocity scaling (CSVR) thermostat was employed to maintain a temperature of 80 °C for Mo and 182 °C for W (the experimental temperatures). The total energy was converged to ± 1.2 kcal/mol for the average energy of the last 500 fs. A final equilibration of 100 fs was then performed using M06-L/DZVP-ALL/GTH-DZVP-SR-MOLOPT[Mo and W] with the GAPW and GTH-MGGA-q14 pseudopotentials. The M06-L method and these pseudopotentials were chosen due to the very large system size. We used a 300 Ry cutoff value. Initial velocities were generated using local mode sampling of the transition-state structure in CP2K. These velocities were then added to the solvent velocities from the last step of the DFT equilibration. Trajectories were propagated for ~1000 fs in the forward direction and ~200 fs in the reverse direction using the GAPW method using a 0.75 fs time step with a velocity-Verlet algorithm. One set of explicit solvent trajectories was performed using only the singlet spin state (allowing for unrestricted singlet solutions). A second set of trajectories was performed using mixed energies and forces from both unrestricted singlet and triplet spin states, which we refer to here as a mixed spin trajectory. Truhlar previously demonstrated that a mixed spin model is useful for obtaining structures and energies of organometallic reactions,[62] and we have previously used this approach to successfully model the reaction between and an Fe complex and ethylene. Mixed spin energies and forces were calculated by coupling the energies, gradients, and hessians using the spin-orbit coupling value obtained through a zero-order regular approximation (ZORA) CASSCF/CASPT2/NEVPT2 calculations in ORCA[63] on the MECP geometry. These calculations estimated spin-orbit coupling values of 0.22 kcal/mol for Mo and 0.49 kcal/mol for W. Inclusion of the mixed spin states provides the ability for the trajectories to take place on a single surface coupled from both singlet to triplet surfaces during the simulation.

Classical molecular dynamics simulations were conducted with GROMACS[64] using a bespoke OPLS force field.[65] Each simulation contained the metal complex along with 718 benzene molecules. For partial atomic charges of the metal complex, we used CM5 charges scaled by a factor of 1.27, which has been shown to work well for condensed-phase simulations.[66] We used the UFF Lennard-Jones parameters for Mo and Si atoms and OPLS parameters for all other atoms.[67] Instead of OPLS bonding parameters for the metal complex we used position restraints. Trajectories were equilibrated for 1 nanosecond (ns) with a 1 fs timestep. We employed the C-rescale pressure coupling algorithm, the Nosé–Hoover thermostat, and the leapfrog integration algorithm for the simulations. See the Supporting Information (SI) for additional computational details.

Results and Discussion

We began by examining the singlet spin state benzene reductive elimination potential energy surface for $[Me_2Si(C_5Me_4)_2]Mo(H)(Ph)$ **1Mo** (Figure 2a), which has never been reported. The reductive coupling transition state, **1Mo**‡, has a forming C-H distance of 1.31 Å (Figure 2c). The Mo-Ph and Mo-H distances were stretched from **1Mo** by 0.19 and 0.12 Å to achieve the **1Mo**‡ structure. The Gibbs barrier for this transition state ($\Delta G^{‡}$) is 29.4 kcal/mol, which is consistent with the 80 °C temperature required for this reaction. B3LYP and ωB97X-D geometries and energies are similar to the M06 structures and energies. IRC calculations indicate that **1Mo**‡ connects to the C-H σ-coordination complex **2Mo** and has a distance of 2.18 Å from the Mo center to the closest hydrogen and a distance of 2.87 Å to the closest carbon. **2Mo**‡ then connects this σ-coordination complex to the π-coordination structure **3Mo** through a twisting motion. The energy surface surrounding **2Mo**, **2Mo**‡, and **3Mo** is very flat with only ~2 kcal/mol separating these structures. From **3Mo** we located a benzene dissociation transition state, **3Mo**‡, that leads to long-range weak complex, **4Mo**. This long-range complex is the result of dispersion interactions between benzene and the cyclopentadienyl ligands. While the enthalpy of **4Mo** is similar to the enthalpy

of **2Mo** and **3Mo** the Gibbs energy decreases substantially. The major difference between **4Mo** and **2Mo** is the distances between the benzene atoms to the metal center. In **4Mo** the relatively long distance between the closest atoms of benzene and the Mo center only provide interaction through weak dispersion-type interactions whereas in **2Mo** the C-H bond of benzene is close enough to the Mo center to allow a small degree of donor/acceptor orbital stabilization. The completely separated structures **5Mo** and benzene require an enthalpy change of 32.2 kcal/mol and a Gibbs energy change of 12.9 kcal/mol.

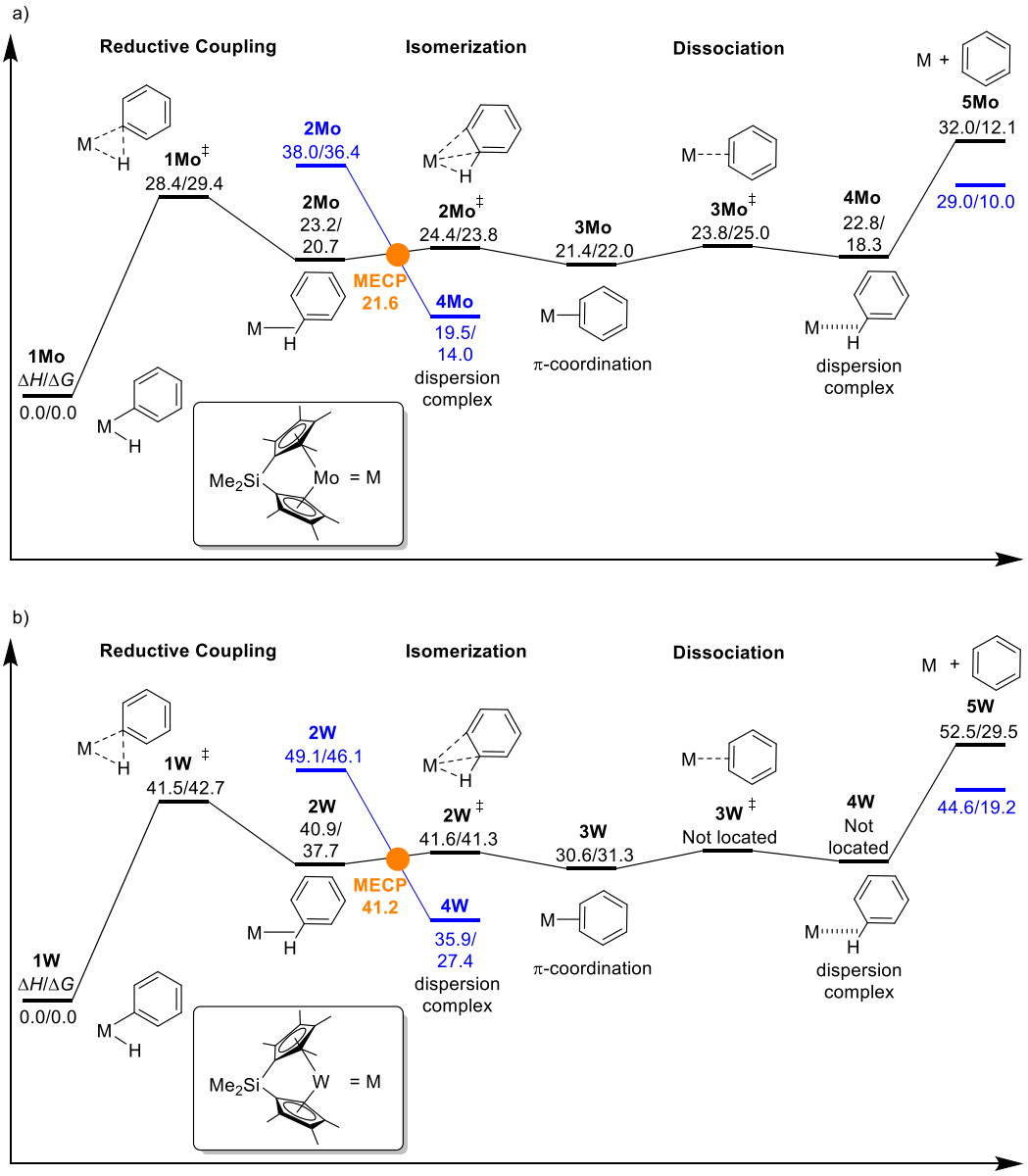

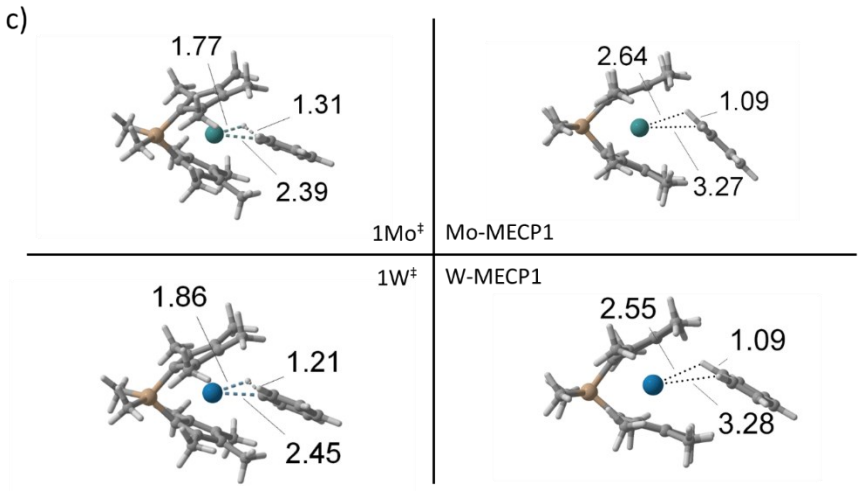

Figure 2. a) M06 DFT potential energy landscapes for reductive elimination of benzene from $[Me_2Si(C_5Me_4)_2]Mo(H)(Ph)$ **1Mo**. Note that for ease of viewing structure-to-structure connections singlet and triplet **4Mo** are shown at different locations. b) M06 DFT potential energy landscapes for reductive elimination of benzene from $[Me_2Si(C_5Me_4)_2]W(H)(Ph)$ **1W**. c) Reductive coupling transition states (**1W**‡ and **1Mo**‡) and **MECP1** structures for Mo and W reactions.

We also examined possible triplet spin state structures related to the singlet spin state structures. The triplet energy of **1Mo**‡ and **2Mo** are more than 10 kcal/mol higher in energy than the singlet spin state. That **2Mo** is this much lower in energy as a singlet is surprising since this structure is only a weak coordination complex. This indicates that the C-H forming reductive coupling process only occurs on the singlet spin state. There are only two structures that have lower energy triplet spin states compared to singlet spin states. These are structures **4Mo** and **5Mo**, which have 3-5 kcal/mol lower triplet energies. This indicates that spin crossover would not occur until benzene begins to be ejected from the Mo metal center. The lower energy **4Mo** suggests that spin crossover is possible even before complete dissociation and therefore we extensively examined the singlet and triplet energy surfaces looking for MECPs. We located **MECP1** that has a geometry in between **2Mo** and **4Mo** (see Figure 1c). The energy of **MECP1** is close to the energy of **2Mo** and likely provides a funnel for spin crossover.

We also explored the singlet and triplet energy surfaces for benzene reductive elimination from $[Me_2Si(C_5Me_4)_2]W(H)(Ph)$ **1W** (Figure 2b). Parkin previously reported only spin restricted singlet B3LYP/6-31G**[LACVP** for W and Si] structures for **1W**‡, **2W**, **2W**‡, and **3W**. Our M06 structures are very similar to Parkin's previously reported structures. The first major difference between the W energy surface and the Mo energy surface is the much larger barrier for the reductive coupling transition state **1W**‡. The 42 kcal/mol barrier is 13 kcal/mol higher than the barrier with Mo and is consistent with the much higher experimental temperature (182 °C) required for benzene reductive elimination. For the singlet surface, we were unable to locate a fully optimized benzene dissociation transition state and weak dispersion structures (**3W**‡ and **4W**). However, similar to Mo, **5W** (the structure with benzene completely eliminated) does have a lower energy triplet spin state, by about 3 kcal/mol, compared to the singlet spin state (an open-shell singlet solution). This prompted us to examine possible MECPs and indeed we located the **MECP1** structure for W.

Because of the relatively flat energy surface surrounding structure **2** we wanted to examine the possibility that this intermediate is nonstatistical using quasiclassical direct dynamics trajectories, which could reveal this intermediate either being bypassed or skipped en route to either formation of the π-complex or benzene dissociation. Quasiclassical NVE trajectories were sampled and propagated starting at **Mo**‡ and **1W**‡. Figure 3a plots the Mo to closest carbon distance as a function of trajectory time for 36 differently sampled trajectories. 0 fs is the transition state. By 175 fs all trajectories show motion beyond

the Mo-C distance of **2Mo**. By 400 fs all the trajectories have reached a M-C distance similar to the dispersion complex **4Mo**. Importantly, about half of the trajectories show complete benzene dissociation with no halting at **2Mo**, **3Mo**, or **4Mo**, and these are highlighted as blue lines. The other half of the trajectories have a peak distance at about 500 fs and then there is slight return of benzene towards the Mo metal center, which are represented by green lines. We have previously labeled this type of trajectory as having paddle ball motion.[68] Nearly all of these returning trajectories result in a structure similar to **4Mo**. Importantly, the π-complex **3Mo** was never formed during the first ps of trajectory time. Overall, these gas-phase trajectories demonstrate the potential energy landscape does not accurately represent the reaction mechanism for this reductive elimination reaction and there can be no stopping at intermediates before benzene dissociation from the Mo complex.

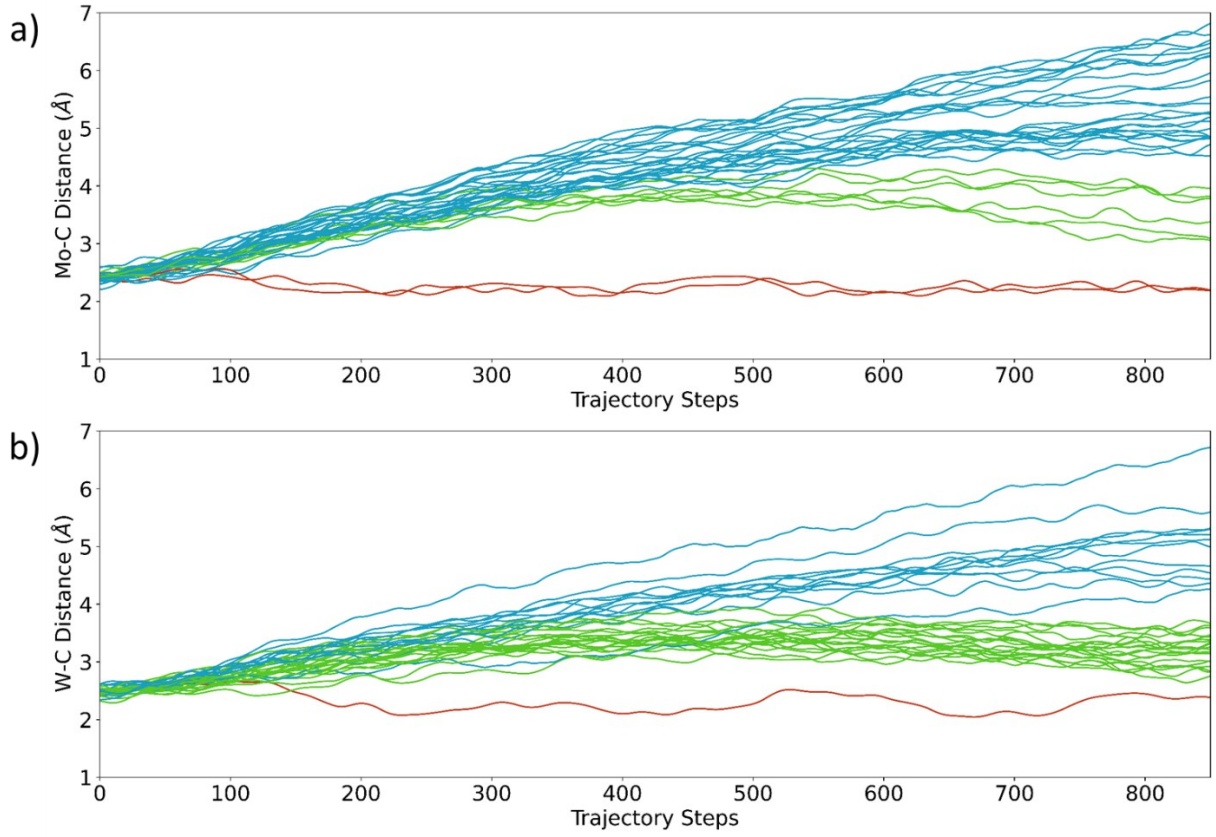

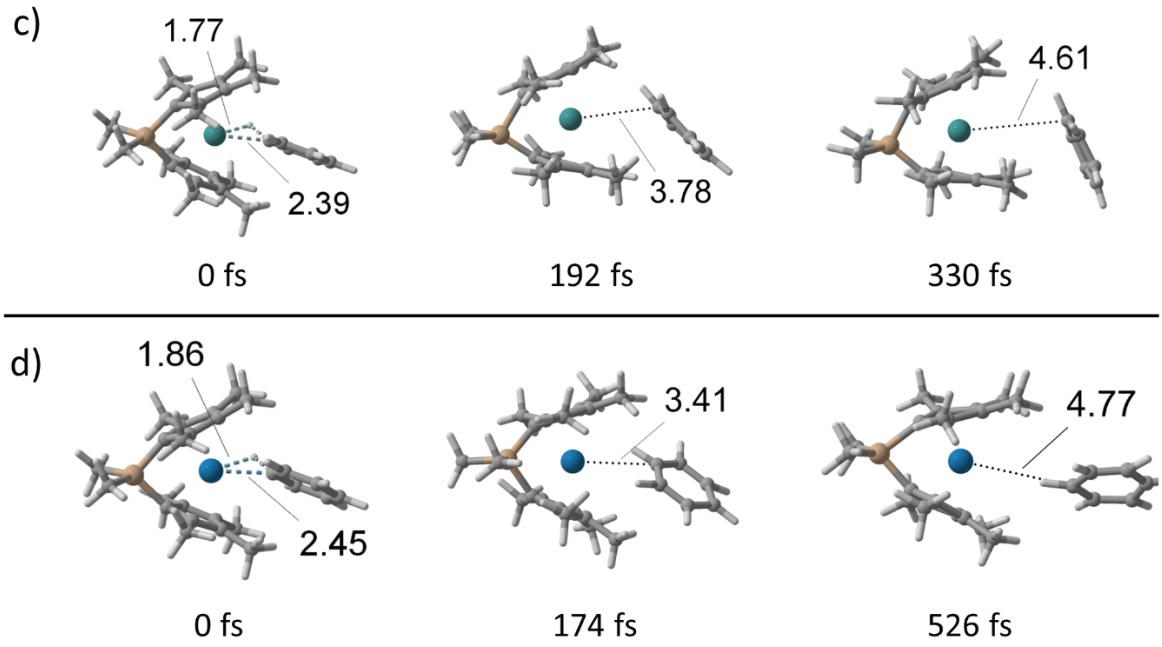

Figure 3. a) Plot of Mo-C distance versus forward trajectory time for gas-phase quasiclassical trajectories starting at **1Mo**‡. Blue line trajectories involve complete benzene dissociation with a final Mo-C distance greater than 4 Å. Green line trajectories involve paddle ball motion with a final Mo-C distance between 2.9 and 4 Å. Red lines involve recrossing back to the Mo hydride structure with a final Mo-C distance less than 2.9 Å. b) Plot of W-C distance versus forward trajectory time for gas-phase quasiclassical trajectories starting at **1W**‡. Blue line trajectories involve complete benzene dissociation with a final W-C distance greater than 4 Å. Green line trajectories involve slight paddle ball motion with a final W-C distance between 2.6 and 4 Å. Red lines involve recrossing back to the Mo hydride structure with a final W-C distance less than 2.6 Å. c) Representative Mo trajectory showing benzene dissociation. d) representative W trajectory showing benzene dissociation.

Figure 3b shows plots of the gas phase W trajectories. For W, similar to Mo, there is again fast passage and no stopping at the C-H σ-complex **2W**. While there are a few W trajectories with complete benzene dissociation trajectories most end in structures most closely related to **4W**, which is somewhat surprising since this structure could not be fully optimized with a potential energy surface search. This indicates that **4W** is a unique dynamic intermediate that is not visible by inspection of the potential energy surface alone, and it is perhaps best labeled as an entropic intermediate.[20] Importantly, none of the trajectories form the π-complex or structures close to the σ-complex. However, while these initial gas-phase trajectories indicate that the reaction mechanism for benzene reductive elimination (at least during the 1 ps time regime) is governed by dynamic effects it is important to clarify that these trajectories did not include explicit solvation and did not include the possibility of spin crossover, and both of these effects might steer the reductive elimination motion.

Explicit solvent (benzene) could have several possible effects on the reductive elimination reaction dynamics of benzene. Solvent could potentially stabilize and reinforce the potential energy surface intermediates, and this could result in a longer-lived C-H σ-coordination intermediate or induce formation of the π-coordination intermediate. Solvent could act as a hard boundary/cage and induce rebound of benzene to reform either the C-H σ-coordination intermediate or the π-coordination intermediate. Alternatively, solvent could facilitate benzene dissociation through stabilizing noncovalent interactions.

After surrounding the transition states **1Mo**‡ and **1W**‡ with a box of 72 benzenes and equilibration with xTB and then DFT, we then propagated trajectories (transition state quasiclassical, solvent classical) for at least 1000 fs. Figure 4a plots the Mo-C distance versus time for 38 explicitly solvated single spin state trajectories starting from **1Mo**‡. Perhaps surprisingly, the trajectories plotted in Figure 4a are very similar to the gas-phase trajectories plotted in Figure 3a. This indicates that explicit solvent does not stabilize or reinforce the potential energy surface intermediates and neither the C-H σ-coordination nor the π-coordination intermediate are formed directly from the reductive coupling transition state. Again, similar to gas-phase trajectories, these singlet spin state explicit solvent trajectories result in a mixture of direct benzene dissociation and some paddle ball motion forming the dispersion type structure.

Figure 4b plots trajectories begun at **1W**‡ and are qualitatively similar to the Mo trajectories. The only major difference is that for W there are a few more recrossing trajectories than the single Mo recrossing trajectory. Overall, these explicit solvent Mo and W trajectories indicate that the C-H σ-coordination complex is a nonstatistical intermediate (and perhaps should not be called an intermediate) and skipped as well as the general direct ejection of benzene without formation of the π-complex.

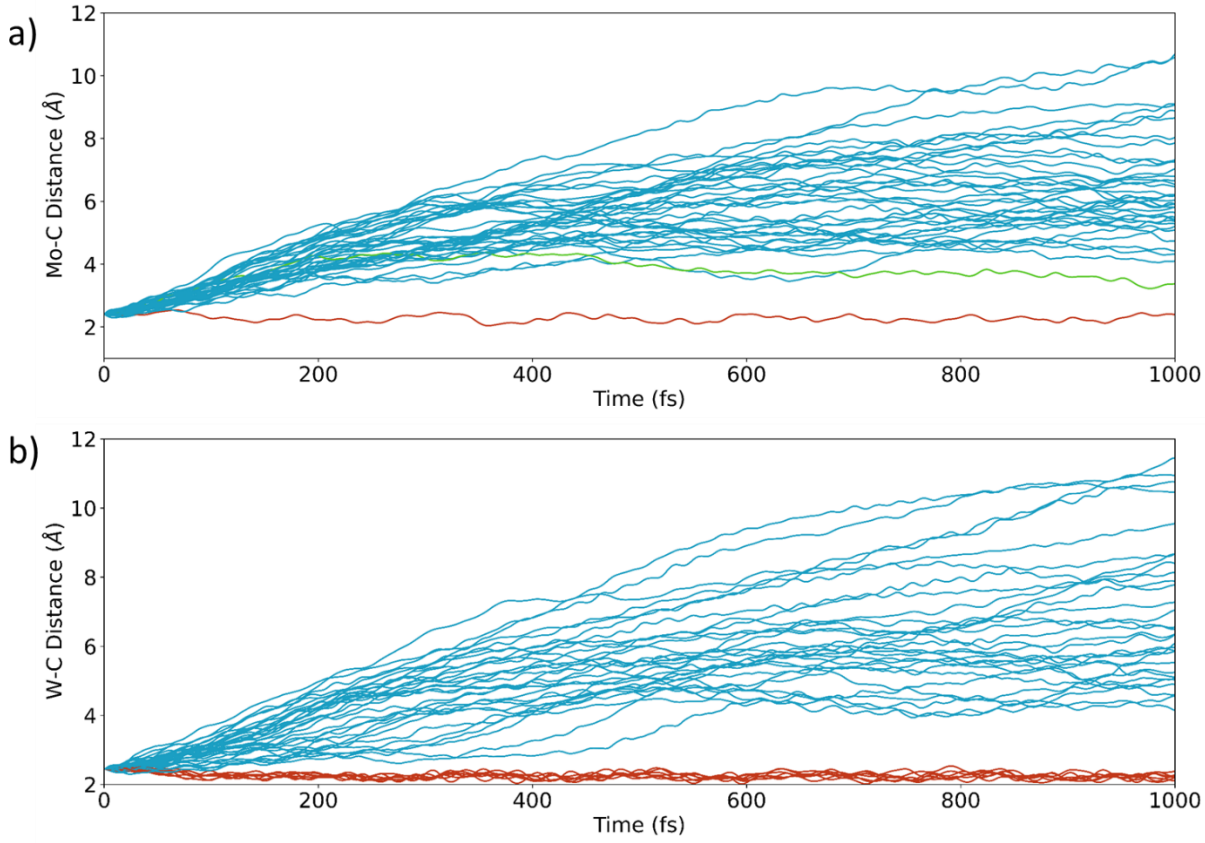

Figure 4. a) Plot of Mo-C distance versus trajectory time for explicit solvent trajectories starting at **1Mo**‡. Blue line trajectories involve complete benzene dissociation. Green line trajectories involve slight paddle ball motion. Red lines involve recrossing back to the Mo hydride structure. b) Plot of W-C distance versus trajectory time for explicit solvent trajectories starting at **1W**‡. Blue line trajectories involve complete benzene dissociation. Green line trajectories involve paddle ball motion. Red lines involve recrossing back to the Mo hydride structure. Trajectories are classified based on the bond distance at the final step shown in the plots. Distances were similar to those of gas phase simulations.

In addition to inclusion of explicit solvent we also wanted to determine the effect of the triplet spin state on reaction dynamics. This was especially important to consider because the MECP has a

geometry very similar to **2Mo/W** and **5W** with benzene fully dislodged has a lower energy triplet spin state. We speculated that access to the triplet spin state either does not significantly influence the outcome of trajectories or enhances benzene dissociation since for most structures since the triplet state of the W/Mo cores is much less stabilizing with interaction of benzene than the corresponding singlet spin state core structures. Therefore, we launched another batch of explicitly solvated trajectories starting at **1Mo**‡ but using a mixed spin electronic configuration. Briefly, during trajectories energies and forces are calculated by mixing unrestricted singlet and unrestricted triplet spin states. This provides effective spin crossover if the system changes from a configuration dominated by the singlet spin state to a configuration dominated by the triplet spin state (see the SI for details), however this does not provide any consideration of probability of spin state change. Figure 5a plots the Mo-C distance versus time for 28 trajectories using this mixed spin approach. **1Mo**‡ is quasiclassical and the benzene solvent has classical sampling. Similar to the singlet spin only trajectories all non-recrossing trajectories resulted in rapid passing through the C-H σ-coordination structure **2Mo** and completely bypassing the π-coordination complexes **3Mo**. For most trajectories only about 100 fs is required for benzene to be ejected from the Mo metal center. Importantly, all trajectories show spin crossover with change from a dominant singlet spin state to a dominant triplet spin state. Figure 6a provides a histogram of the time when spin crossover occurs to a dominant triplet spin state. Figure 6c plots a representative trajectory and the singlet and triplet spin state contributions. Overall, the mixed spin trajectories provide a similar mechanistic vantage point as the singlet spin only trajectories.

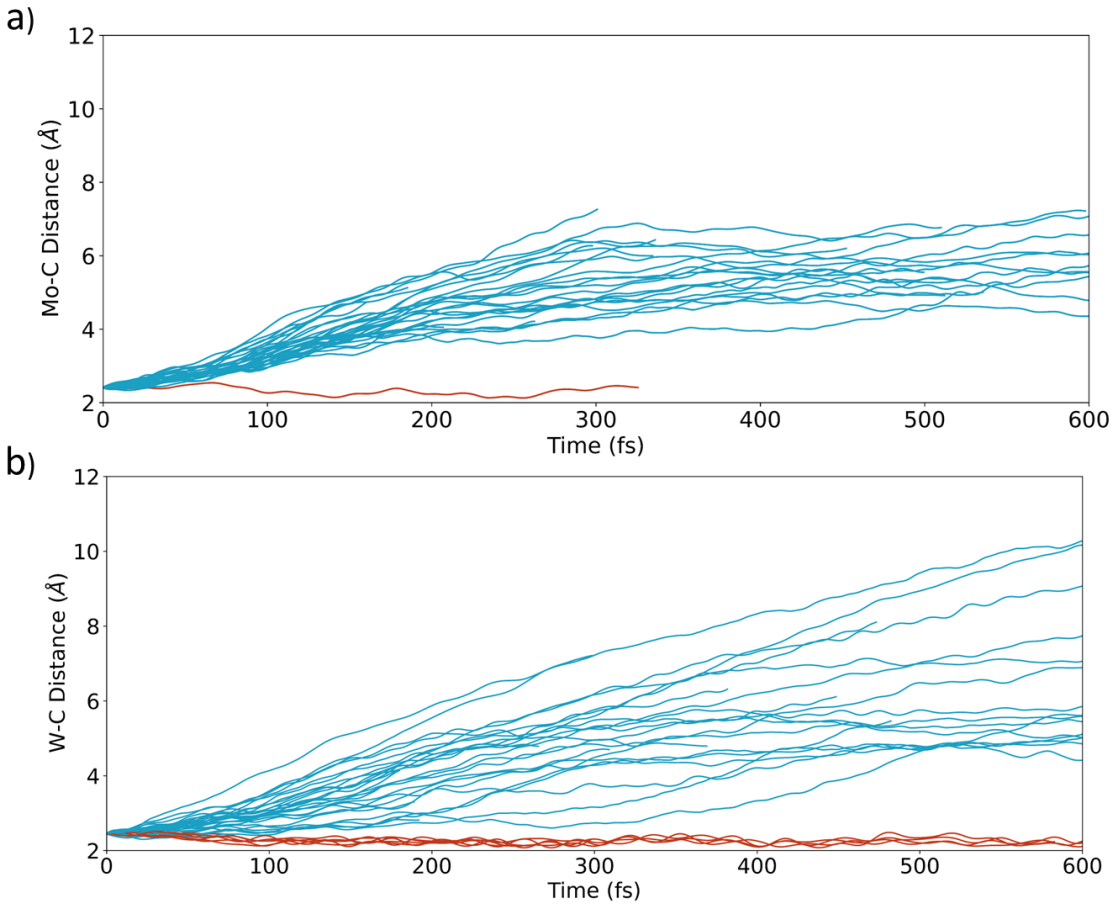

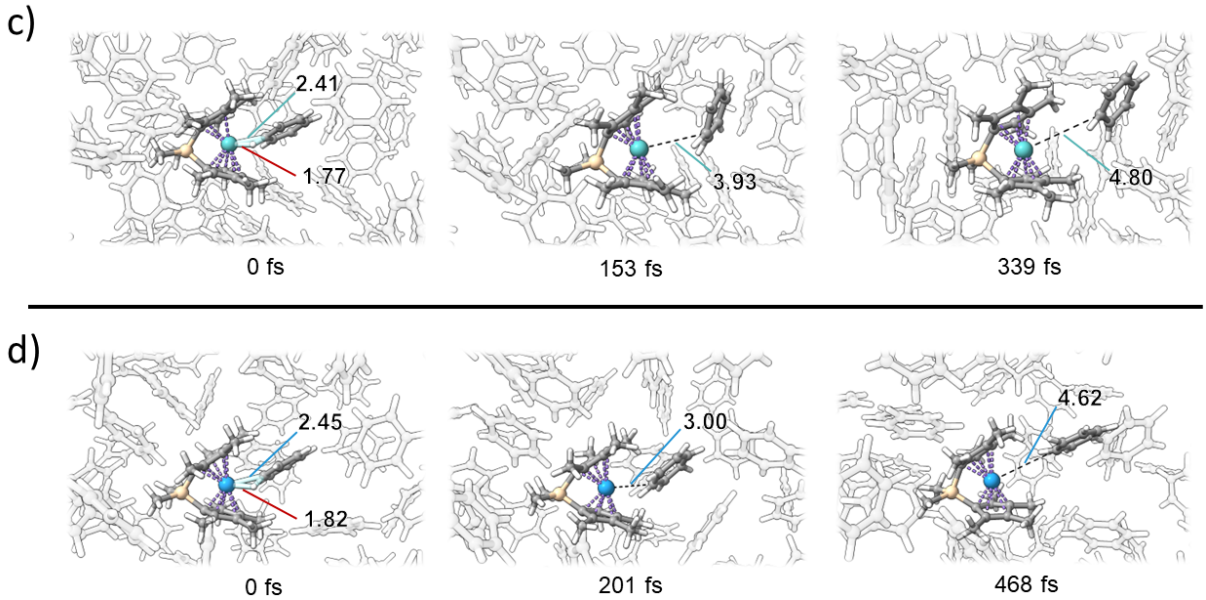

Figure 5. a) Plot of Mo-C distance versus trajectory time (starting at **1Mo**‡) for explicit solvent trajectories propagated as an adiabatic mixture of singlet and triplet spin states. Blue line trajectories involve complete benzene dissociation. Red lines involve recrossing back to the Mo hydride structure. b) Plot of W-C distance versus trajectory time (starting at **1W**‡) for explicit solvent trajectories propagated as an adiabatic mixture of singlet and triplet spin states. Blue line trajectories involve complete benzene dissociation. Red lines involve recrossing back to the Mo hydride structure. c) Snapshots of a representative explicitly solvated mixed spin state trajectory for **1Mo**‡. d) Snapshots of a representative explicitly solvated mixed spin state trajectory for **1W**‡.

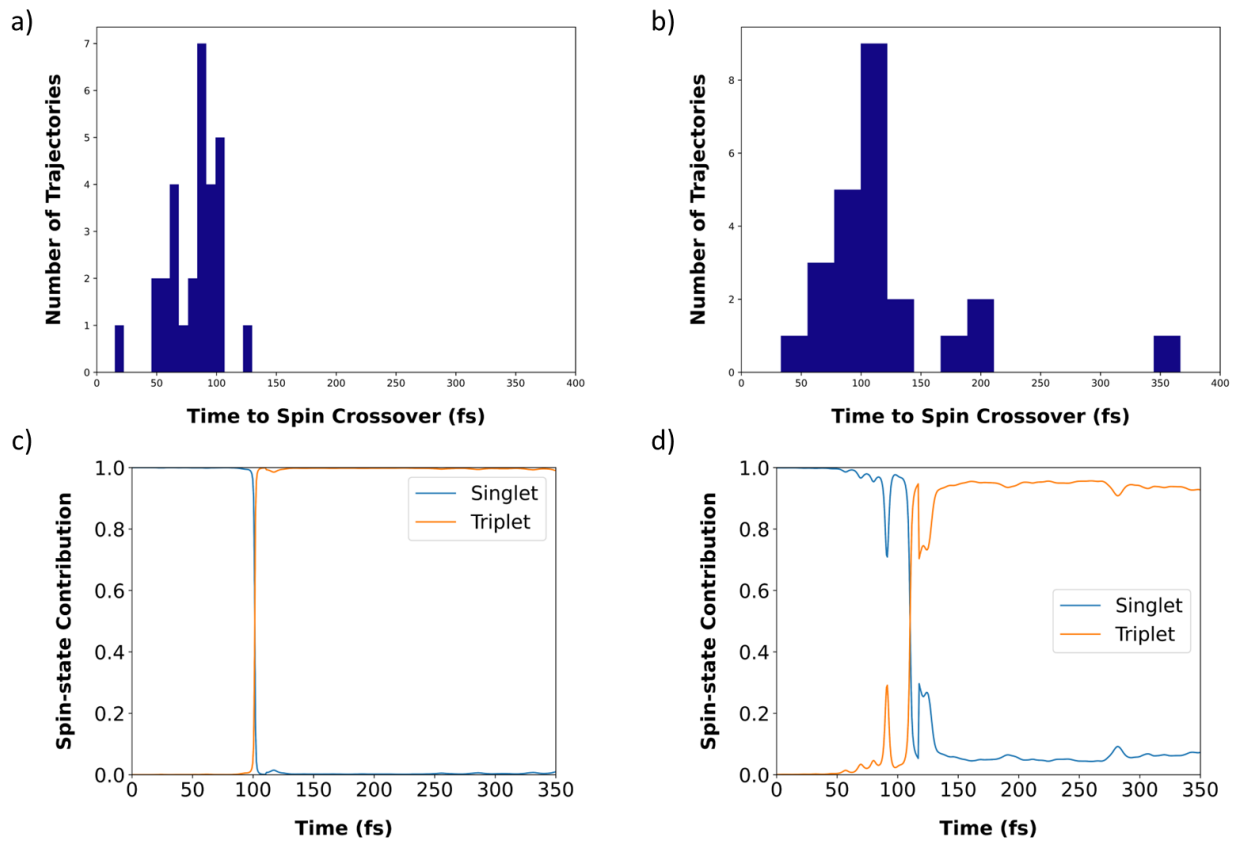

Figure 6. a) Histogram of timing for change from dominant singlet spin state to dominant triplet spin state for trajectories started from **1Mo**‡. b) Histogram of timing for change from dominant singlet spin state to dominant triplet spin state for trajectories started from **1W**‡. c) Plot of spin state contribution for a representative **1Mo**‡ trajectory. d) Plot of spin state contribution for a representative **1W**‡ trajectory.

The gas-phase, explicit solvent, and mixed spin trajectories all point to a mechanistic situation where the initial reductive coupling transition state is dynamically a reductive elimination transition state in the sense that it leads mostly to a solvent caged spin flipped intermediate where the benzene is outside the coordination sphere of the Mo and W metal centers and either there is no directly interaction with the metal complex or there is a noncovalent type interaction (dispersion-type complex). This is fundamentally a different mechanism than three separate reaction steps that include reductive coupling, isomerization, and dissociation.

The discovery of this dynamical mechanism at the ps time scale prompted us to reconsider the interpretation of the KIE values measured for **1Mo** and **1W**, specifically a normal k_H/k_D KIE value for Mo and an inverse k_H/k_D KIE value for W. As outlined in the introduction, Parkin rationalized the normal value for Mo based on rate limiting reductive coupling and the inverse value for W based on formation of an intermediate (presumably the σ-coordination or π-coordination) after reductive coupling followed by rate limiting benzene dissociation.[53] While it is clear that for **1Mo** the reductive coupling transition state fully determines the normal KIE value we wondered if it was possible that for **1W** the reductive coupling transition state might partially contribute to the measured inverse KIE value. This possibility is bolstered by the static potential energy surfaces where all the stationary points located after **1Mo**‡ and **1W**‡ have Gibbs energies that are lower than these transition-state structures. However, as is well known the Gibbs energy of **5Mo**/**W** and separated benzene is likely to slightly too low in energy due to an overestimation of translational entropy. Additionally, the transition-state structure for **1Mo**‡ and **1W**‡ are probably best interpreted as late along the reaction coordinate for bond formation.

We calculated k_H/k_D KIE values comparing $[Me_2Si(C_5Me_4)_2]M(H)(C_6H_5)$ versus $[Me_2Si(C_5Me_4)_2]M(D)(C_6D_5)$. For Mo, using **1Mo** and **1Mo**‡ structures with only changes in zero-point energies gave a normal KIE value of 1.32. Using enthalpy and Gibbs energies gives values of 1.11 and 1.51, respectively. Quasi-harmonic corrections do not significantly change these values. Interestingly, using the Bigeleisen-Meyer approach gave a higher value of 2.02. Both Wigner and Bell tunneling corrections, using the imaginary frequency for the reaction coordinate, have the effect of increasing the KIE value by 0.2-0.3 (see SI). Importantly, all these approaches to estimating the KIE for **1Mo** provide a normal KIE value, but the value is generally slightly higher than the experimental value of 1.1. It is useful to note that this comparison of calculated KIE values versus experiment is inherently qualitative due to the non-consideration of several other factors that influence KIEs, such as moments of inertia.[3,53,54]

For W, using **1W** and **1W**‡ structures with only changes in zero-point energies gave an inverse KIE value of 0.91. Enthalpy and Gibbs energies gave values of 0.83 and 0.96. Similar to Mo, quasi-harmonic corrections do not change these values and the Bigeleisen-Meyer approach gave a value of 0.95. Wigner and Bell tunneling corrections change these KIE values by only 0.01, which is much less than the change for the Mo structures. Importantly, the KIE values are calculated with all of these methods are inverse. They are only slightly inverse likely because the calculated KIE values are generally overestimated compared to experiment, which was also shown to be the case for Mo. This calculated inverse KIE value for W is consistent with the significantly later transition-state position of **1W**‡ versus **1Mo**‡. Importantly, however, this calculated inverse KIE for **1W**‡ does not guarantee that it is the dominant contribution to the experimentally measured KIE, especially because it is of a lower magnitude than the experimental value. Three general scenarios exist. 1) The experimentally measured inverse KIE does reflect the inverse value for **1W**‡. 2) The experimentally measured inverse KIE is the result of solvent caged intermediate that then goes on to exchange with solvent (see later discussion). 3) The experimentally measured inverse KIE is a composite of the inverse value for **1W**‡ and benzene exchange with solvent. Regardless of which of these scenarios is correct it is important to realize that all the steps involved in benzene reductive elimination with the W metal center give an inverse KIE value.

Once the solvent caged intermediate is formed there are two major possibilities for subsequent reaction steps. The first possibility is that the ejected benzene could rebound back to the metal complex and undergo oxidative addition to reform the metal phenyl hydride complex or could only form either of the of the coordination structures (σ or π). In this scenario the solvent caged intermediate is likely either in full or partial equilibrium with the starting metal phenyl hydride structure. Consistent with this thinking, we launched 20 from a solvent caged like structure where benzene began the trajectory about 6 Å away from the metal center and with random initial velocities. As expected, several trajectories formed either the dispersion structure or the π-coordination structure within about 2 ps. No trajectories resulted in C-H bond cleavage because trajectories were initialized with the energy of about structure **4**.

The second possibility is that the benzene stays solvent caged until there is benzene-for-solvent exchange. To examine the lifetime of the caged structure versus exchange with solvent we carried out classical molecular dynamics simulations where the Mo complex was restrained and next to the caged benzene. Figure 7 shows periodic snapshots of one of the classical molecular dynamics simulations. These simulations showed that the caged intermediate has an average lifetime in the range of >100 ps, with many pairs surviving for several hundred picoseconds. While these force field-based simulations cannot investigate reaction with the metal complex versus cage escape, the long lifetime does suggest that cage escape is likely relatively slow and there may indeed be cage induced rebound. In this scenario there is equilibration between the metal phenyl hydride intermediate and the caged intermediate with slow cage escape, and this has the potential for explaining an inverse KIE value.

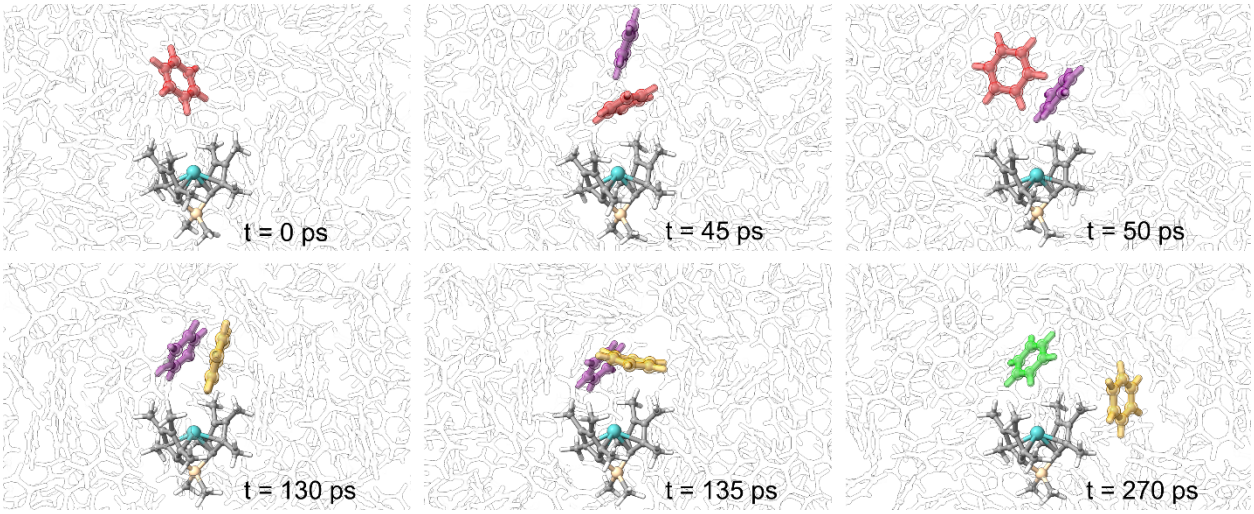

Figure 7. Snapshots of classical molecular dynamics simulations of the caged intermediate and exchange with solvent (benzene). The red highlighted benzene is the initial solvent caged benzene. At 45 and 50 ps the caged benzene is swapped by a purple solvent benzene.

Conclusions

Gas-phase, explicit solvent, and mixed spin state trajectories all indicate that for benzene reductive elimination from Mo and W cyclopentadienyl phenyl hydride complexes involves a dynamic mechanism that initially at the ps time scale skips the C-H σ-coordination structure and bypasses the π-coordination structure and first leads to a spin flipped solvent caged intermediate. This dynamic mechanism is different from the energy landscape mechanistic sequence where the reductive coupling transition state leads to the σ-coordination and then π-coordination structures. This new dynamical mechanism stimulated the reconsideration of the benzene reductive elimination k_H/k_D KIE values for Mo and W comparing $[Me_2Si(C_5Me_4)_2]M(H)(C_6H_5)$ versus $[Me_2Si(C_5Me_4)_2]M(D)(C_6D_5)$. Based on the C-H forming transition state, using three different estimates, calculations revealed that Mo has a normal KIE value and W has a slightly inverse KIE value. Classical molecular dynamics simulations were then used to estimate the lifetime of the caged intermediate, which is between 200-400 picoseconds. This indicates that if the η^2-π-coordination intermediate is formed it occurs only after first formation of the solvent caged intermediate. Overall, these dynamics trajectories combined with KIE calculations provide three possibilities for understanding the normal KIE value for Mo and inverse KIE value for W. 1) The experimentally measured KIE values reflect the normal value for **1Mo**‡ and inverse value for **1W**‡. 2) The measured inverse KIE for W is the result of a solvent caged intermediate that then slowly goes on to exchange with solvent. In this scenario there is the possibility of equilibrium with the metal phenyl hydride. 3) The measured inverse KIE for W is a composite of the inverse value for **1W**‡ and the second step of the solvent caged intermediate undergoing benzene-for-solvent exchange. Regardless of which of these scenarios is most correct it is important to realize that all the steps involved in benzene reductive elimination with the W metal center contribute to an inverse KIE value.

Associated Content

Supporting Information

The Supporting Information is available free of charge.

Xyz coordinates and absolute energy of optimized DFT structures, representative initial trajectory conditions, further details about explicit solvation and trajectories, mixed spin trajectories, and force fields.

Acknowledgements

We thank the Office of Research Computing at BYU for computational resources. We acknowledge and the United States National Science Foundation Chemical Structure, Dynamics, and Mechanisms B (CSDM-B) Program for support under award CHE-2244799.

Author Information

Corresponding Author

Daniel H. Ess - Department of Chemistry and Biochemistry, Brigham Young University, Provo, Utah, 84604, United States; Email: dhe@byu.edu

Author

Josh Wheeler - Department of Chemistry and Biochemistry, Brigham Young University, Provo, Utah, 84604, United States

Anthony J. Schaefer - Department of Chemistry and Biochemistry, Brigham Young University, Provo, Utah, 84604, United States

References

1. Fukui, K. The Path of Chemical Reactions – The IRC Approach. *Acc. Chem. Res.* **1981**, 14, 363–368.
2. Niu, S.; Hall, M. B. Theoretical Studies on Reactions of Transition-Metal Complexes. *Chem. Rev.* **2000**, *100*, 353–405.
3. Gómez-Gallego, M.; Sierra, M. A. Kinetic Isotope Effects in the Study of Organometallic Reaction Mechanisms. *Chem. Rev.* **2011**, *111*, 4857–4963.
4. Eyring, H. The Activated Complex in Chemical Reactions. *J. Chem. Phys.* **1935**, *3*, 107–115.
5. Laidler, K. J.; King, M. C. The Development of Transition-State Theory. *J. Phys. Chem.* **1983**, *87*, 2657–2664.
6. Truhlar, D. G. Garrett, B. C.; Klippenstein, S. J. Current Status of Transition-State Theory. *J. Chem. Phys.* **1996**, *100*, 12771–12800.
7. Carpenter, B. K. Dynamic behavior of organic reactive intermediates. *Angew. Chem. Int. Ed.* **1998**, *37*, 3340–3350.
8. Carpenter, B. K. Nonstatistical Dynamics in Thermal Reactions of Polyatomic Molecules. *Annu. Rev. Phys. Chem.* **2005**, *56*, 57–89.
9. Carpenter, B. K. Energy Disposition in Reactive Intermediates *Chem. Rev.* **2013**, *113*, 7265–7286.
10. Raff, L. M.; Thompson, D. L. in *Theory of Chemical Reaction Dynamics*, Ed. M. Baer (CRC, Boca Raton, FL, 1985).
11. Bolton, K.; Hase, W. L.; Peslherbe, G. H. in *Modern Methods for Multidimensional Dynamics Computation in Chemistry*, Ed. D. L. Thompson (World Scientific, Singapore, 1998) 143.
12. Carpenter, B. K. Nonstatistical Dynamics in Thermal Reactions of Polyatomic Molecules. *Annu. Rev. Phys. Chem.* **2005**, *56*, 57–89.
13. Lourderaj, U.; Park, K.; Hase, W. L. Classical trajectory simulations of post-transition state dynamics. *Int. Rev. Phys. Chem.* **2009**, *113*, 2236–2253.
14. Paranjothy, M.; Sun, R.; Zhuang, Y.; Hase, W. L. Direct Chemical Dynamics Simulations: Coupling of Classical and Quasiclassical Trajectories with Electronic Structure Theory. *Wiley Interdiscip. Rev. Comput. Mol. Sci.* **2013**, *3*, 296–316.
15. Ma X.; Hase, W. L. Perspective: chemical dynamics simulations of non-statistical reaction dynamics. *Philos. Trans. R. Soc., A*, **2017**, *375*, 20160204.
16. Spezia, R.; Martínez-Nuñez, E.; Vazquez, S.; Hase, W. L. Theoretical and computational studies of non-equilibrium and non-statistical dynamics in the gas phase, in the condensed phase and at interfaces. *Phil. Trans. R. Soc. A* **2017**, *375*, 20170035.
17. Yamataka, H. Molecular dynamics simulations and mechanism of organic reactions: non-TST behaviors. *Adv. Phys. Org. Chem.* **2010**, *44*, 173–222.

18. Doubleday, C. Jr.; McIver, J. W. Jr.; Page, M. Singlet biradicals as intermediates. Canonical variational transition-state theory results for trimethylene. *J. Phys. Chem.* **1988**, *92*, 4367–4371.
19. Gonzalez-James, O. M.; Kwan; E. E.; Singleton, D. A. Entropic Intermediates and Hidden Rate-Limiting Steps in Seemingly Concerted Cycloadditions. Observation, Prediction, and Origin of an Isotope Effect on Recrossing. *J. Am. Chem. Soc.* **2012**, *134*, 1914–1917.
20. Yang, Z.; Jamieson, C. S.; Xue, X.-S.; Garcia-Borràs, M.; Benton, T.; Dong, X.; Liu F.; Houk, K. N. Mechanisms and Dynamics of Reactions Involving Entropic Intermediates. *Trends in Chemistry*, **2019**, *1*, 22–34.
21. Ess, D. H.; Wheeler, S. E.; Iafe, R. G.; Xu, L.; Celebi-Olcum, N.; Houk, K. N. Bifurcations on Potential Energy Surfaces of Organic Reactions. *Angew. Chem. Int. Ed.* **2008**, *47*, 7592–7601.
22. Hare, S. R.; Tantillo, D. J. Post-transition state bifurcations gain momentum – current state of the field. *Pure Appl. Chem.* **2017**, *89*, 679–698.
23. Karmakar, S.; Keshavamurthy, S. Intramolecular vibrational energy redistribution and the quantum ergodicity transition: a phase space perspective. *Phys. Chem. Chem. Phys.* **2020**, *22*, 11139–11173.
24. Singleton, D. A.; Hang, C.; Szymanski M. J.; Greenwald, E. E. A New Form of Kinetic Isotope Effect. Dynamic Effects on Isotopic Selectivity and Regioselectivity. *J. Am. Chem. Soc.*, **2003**, *125*, 1176–1177.
25. Lopez, J. G.; Vayner, G.; Lourderaj, U.; Addepalli, S. V.; Kato, S.; deJong, W. A.; Windus, T. L.; Hase, W. L. A Direct Dynamics Trajectory Study of F^- + CH_3OOH Reactive Collisions Reveals a Major Non-IRC Reaction Path. *J. Am. Chem. Soc.* **2007**, *129*, 9976–9985.
26. Manikandan, P.; Zhang, J.; Hase, W. L. Chemical Dynamics Simulations of X^- + $CH_3Y \rightarrow XCH_3 + Y^-$ Gas-Phase S_N2 Nucleophilic Substitution Reactions. Nonstatistical Dynamics and Nontraditional Reaction Mechanisms. *J. Phys. Chem. A* **2012**, *116*, 3061–3080.
27. Bogle, X. S.; Singleton, D. A. Dynamic Origin of the Stereoselectivity of a Nucleophilic Substitution Reaction. *Org. Lett.* **2012**, *14*, 2528–2531.
28. Xie, J.; Otto, R.; Mikosch, J.; Zhang, J.; Wester, R.; Hase, W. L. Identification of Atomic-Level Mechanisms for Gas-Phase X^- + CH_3Y S_N2 Reactions by Combined Experiments and Simulations. *Acc. Chem. Res.* **2014**, *47*, 2960–2969.
29. Bailey, J. O.; Singleton, D. A. Failure and Redemption of Statistical and Nonstatistical Rate Theories in the Hydroboration of Alkenes. *J. Am. Chem. Soc.* **2017**, *139*, 15710–15723.
30. Chen, Z.; Nieves-Quinones, Y.; Waas, J. R.; Singleton, D. A. Isotope Effects, Dynamic Matching, and Solvent Dynamics in a Wittig Reaction. Betaines as Bypassed Intermediates. *J. Am. Chem. Soc.* **2014**, *136*, 13122–13125.
31. Glowacki, D. R.; Marsden, S.; Pilling, M. J. Significance of Nonstatistical Dynamics in Organic Reaction Mechanisms: Time-Dependent Stereoselectivity in Cyclopentyne−Alkene Cycloaddition. *J. Am. Chem. Soc.* **2009**, *131*, 13896–13897.
32. Wang, Z.; Hirschi, J. S.; Singleton, D. A. Recrossing and Dynamic Matching Effects on Selectivity in a Diels-Alder Reaction. *Angew. Chem. Int. Ed. Engl.* **2009**, *48*, 9156–9159.
33. Yu, P.; Chen, T. Q.; Yang, Z.; He, C. Q.; Patel, A.; Lam, Y.-h.; Liu, C.-Y.; Houk, K. N. Mechanisms and Origins of Periselectivity of the Ambimodal [6 + 4] Cycloadditions of Tropone to Dimethylfulvene. *J. Am. Chem. Soc.* **2017**, *139*, 8251–8258.
34. Biswas, B.; Collins, S. C.; Singleton, D. A. Dynamics and a Unified Understanding of Competitive [2, 3]- and [1,2]-Sigmatropic Rearrangements Based on a Study of Ammonium Ylides. *J. Am. Chem. Soc.* **2014**, *136*, 3740–3743.
35. Hare, S. R.; Li, A.; D. J. Tantillo, Post-transition state bifurcations induce dynamical detours in Pummerer-like reactions. *Chem. Sci.* 2018, **9**, 8937–8945.
36. Hong, Y. J.; Tantillo, D. J. Biosynthetic consequences of multiple sequential post-transition-state bifurcations. *Nat. Chem.* **2014**, *6*, 104–111.
37. Doubleday, C.; Suhrada, C. P.; Houk, K. N. Dynamics of the Degenerate Rearrangement of Bicyclo[3.1.0]hex-2-ene. *J. Am. Chem. Soc.* **2006**, *128*, 90–94.
38. Doubleday, C.; Li, G.; Hase, W. L. Dynamics of the biradical mediating vinylcyclopropane-cyclopentene rearrangement. *Phys. Chem. Chem. Phys.* **2002**, *4*, 304–312.

39. Doubleday, C.; Nendel, M.; Houk, K. N.; Thweatt, D.; Page, M. Direct Dynamics Quasiclassical Trajectory Study of the Stereochemistry of the Vinylcyclopropane-Cyclopentene Rearrangement. *J. Am. Chem. Soc.* **1999**, *121*, 4720–4721.
40. Ess, D. H. Quasiclassical Direct Dynamics Trajectory Simulations of Organometallic Reactions. *Acc. Chem. Res.* **2021**, *54,* 4410–4422.
41. Rowley, C. N.; Woo, T. K. A Path Sampling Study of Ru-Hydride-Catalyzed H_2 Hydrogenation of Ethylene. *J. Am. Chem. Soc.* **2008**, *130*, 7218–7219.
42. Zhang, L.; Wang, Y.; Yao, Z-J.; Wang, X.; Yu, Z-X. Kinetic or Dynamic Control on a Bifurcating Potential Energy Surface? An Experimental and DFT Study of Gold-Catalyzed Ring Expansion and Spirocyclization of 2-Propargyl-*β*-tetrahydrocarbolines. *J. Am. Chem. Soc.* **2015**, *137*, 13290–13300.
43. Kpante, M.; Wolf, L. M. Pathway Bifurcations in the Activation of Allylic Halides by Palladium and Their Influence on the Dynamics of η^1 and η^3 Allyl Intermediates. *J. Org. Chem.* **2021**, *86*, 9637-9650.
44. Hare, S. R.; Tantillo, D. J. Cryptic post-transition state bifurcations that reduce the efficiency of lactone-forming Rh-carbenoid C–H insertions. *Chem. Sci.* **2017**, *8*, 1442–1449.
45. Guo, W.; Hare, S. R.; Chen. S.-S.; Saunders, C.; Tantillo, D. J. C-H Insertion in Dirhodium Tetracarboxylate-Catalyzed Reactions Despite Dynamical Tendencies Toward Fragmentation – Implications for Reaction Efficiency and Catalyst Design. *J. Am. Chem. Soc.* **2022**, *144*, 17219–17231.
46. Guo, W.; Tantillo, D. J. Running Wild through Dirhodium Tetracarboxylate-Catalyzed Combined CH(C)-Functionalization/Cope Rearrangement Landscapes: Does Post-Transition-State Dynamic Mismatching Influence Product Distributions?. *J. Am. Chem. Soc.* **2024**, *146*, 7039–7051.
47. Ye, L.; Wang, Y.; Aue, G. H.; Zhang, L. Experimental and Computational Evidence for Gold Vinylidenes: Generation from Terminal Alkynes via a Bifurcation Pathway and Facile C-H Insertions. *J. Am. Chem. Soc.* **2012**, *134*, 31–34.
48. Fructos, M. R.; Besora, M.; Braga, A. A. C.; Díaz-Requejo, Maseras, F.; Pérez, P. J. Mechanistic studies on gold-catalyzed direct arene C–H bond functionalization by carbene insertion: the coinage-metal effect. *Organometallics* **2017**, *36*, 172–179.
49. Pu, M.; Nielsen, C. D.-T.; Senol, E.; Sperger, T.; Schoenebeck, F. Post-Transition-State Dynamic Effects in the Transmetalation of Pd(II)-F to Pd(II)-CF_3. *JACS Au* 2024, **4**, 263–275.
50. Yuan, M.; Song, Z.; Badir, S. O.; Molander, G. A.; Gutierrez, O. On the Nature of $C(sp^3)$–$C(sp^2)$ Bond Formation in Nickel-Catalyzed Tertiary Radical Cross-Couplings: A Case Study of Ni/Photoredox Catalytic Cross-Coupling of Alkyl Radicals and Aryl Halides. *J. Am. Chem. Soc.* **2020**, *142*, 7225–7234.
51. Yang, B.; Schouten, A.; Ess, D. H. Direct Dynamics Trajectories Reveal Nonstatistical Coordination Intermediates and Demonstrate that σ and π-Coordination Are Not Required for Rhenium(I)-Mediated Ethylene C−H Activation. *J. Am. Chem. Soc.* **2021**, *143*, 8367–8374.
52. Smith, J. A.; Schouten, A.; Wilde, J. H.; Westendorff, K. S.; Dickie, D. A.; Ess, D. H.; Harmen, W. D. Experiments and Direct Dynamics Simulations Reveal a Network of Reaction Pathways for Tungsten η^2-Arene - Aryl Hydride Equilibria. *J. Am. Chem. Soc.* **2020**, *142*, 16437–16454.
53. Churchill, D. G.; Janak, K. E.; Wittenberg, J. S.; Parkin, G. Normal and Inverse Primary Kinetic Deuterium Isotope Effects for C-H Bond Reductive Elimination and Oxidative Addition Reactions of Molybdenocene and Tungstenocene Complexes: Evidence for Benzene π-Complex Intermediates. *J. Am. Chem. Soc.* **2003**, *125*, 1403–1420.
54. Janak, K. E.; Churchill, D. G.; Parkin, G. Computational evidence that the inverse kinetic isotope effect for reductive elimination of methane from a tungstenocene methyl-hydride complex is associated with the inverse equilibrium isotope effect for formation of a σ-complex intermediate. *Chem. Commun.* **2003**, 22–23.
55. Gaussian 16, Revision B.01, Frisch, M. J.; Trucks, G. W.; Schlegel, H. B.; Scuseria, G. E.; Robb, M. A.; Cheeseman, J. R.; Scalmani, G.; Barone, V.; Petersson, G. A.; Nakatsuji, H.; et al. Gaussian, Inc., Wallingford CT, 2016.
56. Zhao, Y.; Truhlar, D. G. The M06 Suite of Density Functionals for Main Group Thermochemistry, Thermochemical Kinetics, Noncovalent Interactions, Excited States, and Transition Elements: Two New

Functionals and Systematic Testing of Four M06-Class Functionals and 12 Other Functionals. *Theor. Chem. Acc.* **2008**, *120*, 215–241.
57. Ditchfield, R.; Hehre, W. J.; Pople, J. A. Self-Consistent Molecular Orbital Methods. 9. Extended Gaussian-type basis for molecular-orbital studies of organic molecules. *J. Chem. Phys.* **1971**, *54*, 724–728.
58. Hay, P. J.; Wadt, W. R. *Ab Initio* Effective Core Potentials for Molecular Calculations. Potentials for K to Au Including the Outermost Core Orbitals. *J. Chem. Phys.* **1985**, *82*, 299–310.
59. Snyder, J. D.; Hamill, L-A.; Faleumu, K. E.; Schultz, A. R.; Ess. D. H. MECPro Version 1.0.6: Minimum Energy Crossing Program. 2020. https://github.com/DanielEss-lab/mecpro.
60 Smith, K. M.; Poli R.; Harvey, J. N. *Chem. Eur. J.*, **2001**, *7*, 1679–1690.
61. Kühne, T. D. et al. CP2K: An electronic structure and molecular dynamics software package - Quickstep: Efficient and accurate electronic structure calculations. *J. Chem. Phys.* **2020**, *152*, 194103.
62. Yang, B.; Gagliardi, L.; Truhlar, D. G. *Phys. Chem. Chem. Phys.* **2018**, *20*, 4129–4136.
63. Neese, F. The ORCA Program System. *Comput. Mol. Sci.* **2012**, *2*, 73–78.
64. Abraham, M. J.; Murtola, T.; Schulz, R.; Páll, S.; Smith, J. C.; Hess, B.; Lindahl, E. GROMACS: High performance molecular simulations through multi-level parallelism from laptops to supercomputers. *SoftwarX* **2015**, 19–25.
65. Jorgensen, W. L.; Maxwell, D. S.; Tirado-Rives, J. Development and Testing of the OPLS All-Atom Force Field on Conformational Energetics and Properties of Organic Liquids. *J. Am. Chem. Soc.* **1996**, *118*, 11225–11236.
66. Vilseck, J. Z.; Tirado-Rives, J. Jorgensen, W. L. Evaluation of CM5 Charges for Condensed-Phase Modeling. *J. Chem. Theory Comput.* **2014**, *10*, 2802–2812.
67. Jorgensen, W. L.; Severance, D. L. Aromatic-aromatic interactions: free energy profiles for the benzene dimer in water, chloroform, and liquid benzene. *J. Am. Chem. Soc.* **1990**, *112*, 4768–4774.
68. Carlsen, R.; Jenkins, J. R.; Chuang, J.; Pugh, S. L.; Ess, D. H. Paddle Ball Dynamics During Rh-Methyl to Rh-Methane σ-Complex Reductive Elimination. *Organometallics* **2019**, *38*, 2280–2287.

TOC graphic